Dynamically tunable plasmon induced transparency in a graphene-based nanoribbon waveguide coupled with graphene rectangular resonators structure on sapphire substrate

Xu Han,[1] Tao Wang,[1,*] Xiaoming Li,[2] Shuyuan Xiao,[1] and Youjiang Zhu[1]

[1] *Wuhan National Laboratory for Optoelectronics, Huazhong University of Science and Technology, Wuhan 430074, China*

[2] *Key Laboratory of Optoelectronic Devices and Systems of Ministry of Education and Guangdong Province, College of Optoelectronic Engineering, Shenzhen University, Shenzhen 518060, China*

**wangtao@hust.edu.cn*

Abstract: In this paper, we propose dynamically tunable plasmon induced transparency (PIT) in a graphene-based nanoribbon waveguide coupled with graphene rectangular resonators structure on sapphire substrate by shifting the Fermi energy level of the graphene. Two different methods are employed to obtain the PIT effect: one is based on the direct destructive interference between a radiative state and a dark state, the other is based on the indirect coupling through a graphene nanoribbon waveguide. Our numerical results reveal that high tunability in the PIT transparency window can be obtained by altering the Fermi energy levels of the graphene rectangular resonators. Moreover, double PITs are also numerically predicted in this ultracompact structure, comprising series of graphene rectangular resonators. Compared with previously proposed graphene-based PIT effects, our proposed scheme is much easier to design and fabricate. This work not only paves a new way towards the realization of graphene-based integrated nanophotonic devices, but also has important applications in multi-channel-selective filters, sensors, and slow light.

OCIS codes: (240.6680) Surface plasmons; (130.3120) Integrated optics devices; (250.5403) Plasmonics

References and links

1. S. Zhang, D. A. Genov, Y. Wang, M. Liu, and X. Zhang, "Plasmon-induced transparency in metamaterials," Phys. Rev. Lett. **101**(4), 047401 (2008).
2. N. Liu, L. Langguth, T. Weiss, J. Kästel, M. Fleischhauer, T. Pfau, and H. Giessen, "Plasmonic analogue of electromagnetically induced transparency at the Drude damping limit," Nat. Mater. **8**(9), 758–762 (2009).
3. Z. Li, Y. Ma, R. Huang, R. Singh, J. Gu, Z. Tian, J. Han, and W. Zhang, "Manipulating the plasmon-induced transparency in terahertz metamaterials," Opt. Express **19**(9), 8912–8919 (2011).
4. X. Duan, S. Chen, H. Cheng, Z. Li, and J. Tian, "Dynamically tunable plasmonically induced transparency by planar hybrid metamaterial," Opt. Lett. **38**(4), 483–485 (2013).
5. Y. Zhu, X. Hu, Y. Fu, H. Yang, and Q. Gong, "Ultralow-power and ultrafast all-optical tunable plasmon-induced transparency in metamaterials at optical communication range," Sci. Rep. **3**, 2338 (2013).
6. M. Miyata, J. Hirohata, Y. Nagasaki, and J. Takahara, "Multi-spectral plasmon induced transparency via in-plane dipole and dual-quadrupole coupling," Opt. Express **22**(10), 11399–11406 (2014).
7. R. D. Kekatpure, E. S. Barnard, W. Cai, and M. L. Brongersma, "Phase-coupled plasmon-induced transparency," Phys. Rev. Lett. **104**(24), 243902 (2010).
8. H. Lu, X. Liu, and D. Mao, "Plasmonic analog of electromagnetically induced transparency in multi-nanoresonator-coupled waveguide systems," Phys. Rev. A **85**(5), 053803 (2012).
9. X. Han, T. Wang, X. Li, B. Liu, Y. He, and J. Tang, "Dynamically tunable slow light based on plasmon induced transparency in disk resonators coupled MDM waveguide system," J. Phys. D Appl. Phys. **48**(23), 235102 (2015).
10. T. Wang, Y. Zhang, Z. Hong, and Z. Han, "Analogue of electromagnetically induced transparency in integrated plasmonics with radiative and subradiant resonators," Opt. Express **22**(18), 21529–21534 (2014).

#252250 Received 19 Oct 2015; revised 16 Nov 2015; accepted 16 Nov 2015; published 2 Dec 2015

11. G. Lai, R. Liang, Y. Zhang, Z. Bian, L. Yi, G. Zhan, and R. Zhao, "Double plasmonic nanodisks design for electromagnetically induced transparency and slow light," Opt. Express **23**(5), 6554–6561 (2015).
12. Z. Zhang, L. Zhang, H. Li, and H. Chen, "Plasmon induced transparency in a surface plasmon polariton waveguide with a comb line slot and rectangle cavity," Appl. Phys. Lett. **104**(23), 231114 (2014).
13. Z. He, H. Li, S. Zhan, G. Cao, and B. Li, "Combined theoretical analysis for plasmon-induced transparency in waveguide systems," Opt. Lett. **39**(19), 5543–5546 (2014).
14. J. Zhang, W. Bai, L. Cai, Y. Xu, G. Song, and Q. Gan, "Observation of ultra-narrow band plasmon induced transparency based on large-area hybrid plasmon-waveguide systems," Appl. Phys. Lett. **99**(18), 181120 (2011).
15. Z. Chai, X. Hu, Y. Zhu, F. Zhang, H. Yang, and Q. Gong, "Low-power and ultrafast all-optical tunable plasmon-induced transparency in plasmonic nanostructures," Appl. Phys. Lett. **102**(20), 201119 (2013).
16. A. Grigorenko, M. Polini, and K. Novoselov, "Graphene plasmonics," Nat. Photonics **6**(11), 749–758 (2012).
17. M. Jablan, H. Buljan, and M. Soljacic, "Plasmonics in graphene at infrared frequencies," Phys. Rev. B **80**(24), 245435 (2009).
18. A. Vakil and N. Engheta, "Transformation optics using graphene," Science **332**(6035), 1291–1294 (2011).
19. F. Liu and E. Cubukcu, "Tunable omnidirectional strong light-matter interactions mediated by graphene surface plasmons," Phys. Rev. B **88**(11), 115439 (2013).
20. X. Shi, D. Han, Y. Dai, Z. Yu, Y. Sun, H. Chen, X. Liu, and J. Zi, "Plasmonic analog of electromagnetically induced transparency in nanostructure graphene," Opt. Express **21**(23), 28438–28443 (2013).
21. H. Cheng, S. Chen, P. Yu, X. Duan, B. Xie, and J. Tian, "Dynamically tunable plasmonically induced transparency in periodically patterned graphene nanostrips," Appl. Phys. Lett. **103**(20), 203112 (2013).
22. C. Zeng, J. Guo, and X. Liu, "High-contrast electro-optic modulation of spatial light induced by graphene-integrated Fabry-Perot microcavity," Appl. Phys. Lett. **105**(12), 121103 (2014).
23. L. Wang, W. Cai, W. Luo, Z. Ma, C. Du, X. Zhang, and J. Xu, "Mid-infrared plasmon induced transparency in heterogeneous graphene ribbon pairs," Opt. Express **22**(26), 32450–32456 (2014).
24. C. Zeng, Y. Cui, and X. Liu, "Tunable multiple phase-coupled plasmon-induced transparencies in graphene metamaterials," Opt. Express **23**(1), 545–551 (2015).
25. A. Nikitin, F. Guinea, F. Garcia-Vidal, and L. Martin-Moreno, "Edge and waveguide terahertz surface plasmon modes in graphene microribbons," Phys. Rev. Lett. **84**, 161407 (2011).
26. X. Zhu, W. Yan, N. A. Mortensen, and S. Xiao, "Bends and splitters in graphene nanoribbon waveguides," Opt. Express **21**(3), 3486–3491 (2013).
27. J. Christensen, A. Manjavacas, S. Thongrattanasiri, F. H. L. Koppens, and F. J. García de Abajo, "Graphene plasmon waveguiding and hybridization in individual and paired nanoribbons," ACS Nano **6**(1), 431–440 (2012).
28. J. S. Gómez-Díaz and J. Perruisseau-Carrier, "Graphene-based plasmonic switches at near infrared frequencies," Opt. Express **21**(13), 15490–15504 (2013).
29. Z. Huang, L. Wang, B. Sun, M. He, J. Liu, H. Li, and X. Zhai, "A mid-infrared fast-tunable graphene ring resonator based on guided-plasmonic wave resonance on a curved graphene surface," J. Opt. **16**(10), 105004 (2014).
30. B. Zhu, G. Ren, Y. Gao, B. Wu, Q. Wang, C. Wan, and S. Jian, "Graphene plasmons isolator based on non-reciprocal coupling," Opt. Express **23**(12), 16071–16083 (2015).
31. H. Li, L. Wang, J. Liu, Z. Huang, B. Sun, and X. Zhai, "Investigation of the graphene based planar plasmonic filters," Appl. Phys. Lett. **103**(21), 211104 (2013).
32. J. Wang, W. Lu, X. Li, Z. Ni, and T. Qiu, "Graphene plasmon guided along a nanoribbon coupled with a nanoring," J. Phys. D Appl. Phys. **47**(13), 135106 (2014).
33. L. Zhang, J. Yang, X. Fu, and M. Zhang, "Graphene disk as an ultracompact ring resonator based on edge propagating plasmons," Appl. Phys. Lett. **103**(16), 163114 (2013).
34. F. Li, S. D. Jackson, C. Grillet, E. Magi, D. Hudson, S. J. Madden, Y. Moghe, C. O'Brien, A. Read, S. G. Duvall, P. Atanackovic, B. J. Eggleton, and D. J. Moss, "Low propagation loss silicon-on-sapphire waveguides for the mid-infrared," Opt. Express **19**(16), 15212–15220 (2011).
35. E. Palik, *Handbook of Optical Constants of Solids* (Academic, 1991).
36. T. Zhang, L. Chen, B. Wang, and X. Li, "Tunable broadband plasmonic field enhancement on a graphene surface using a normal-incidence plane wave at mid-infrared frequencies," Sci. Rep. **5**, 8443 (2015).
37. L. Wang, W. Li, and X. Jiang, "Tunable control of electromagnetically induced transparency analogue in a compact graphene-based waveguide," Opt. Lett. **40**(10), 2325–2328 (2015).
38. X. Han, T. Wang, X. Li, B. Liu, Y. He, and J. Tang, "Ultrafast and low-power dynamically tunable plasmon-induced transparencies in compact aperture-coupled rectangular resonators," J. Lightwave Technol. **33**(14), 3083–3090 (2015).
39. L. Vicarelli, S. J. Heerema, C. Dekker, and H. W. Zandbergen, "Controlling defects in graphene for optimizing the electrical properties of graphene nanodevices," ACS Nano **9**(4), 3428–3435 (2015).
40. Q. Xu, M. Y. Wu, G. F. Schneider, L. Houben, S. K. Malladi, C. Dekker, E. Yucelen, R. E. Dunin-Borkowski, and H. W. Zandbergen, "Controllable atomic scale patterning of freestanding monolayer graphene at elevated temperature," ACS Nano **7**(2), 1566–1572 (2013).
41. Z. J. Qi, C. Daniels, S. J. Hong, Y. W. Park, V. Meunier, M. Drndić, and A. T. C. Johnson, "Electronic transport of recrystallized freestanding graphene nanoribbons," ACS Nano **9**(4), 3510–3520 (2015).
42. J. Baringhaus, M. Ruan, F. Edler, A. Tejeda, M. Sicot, A. Taleb-Ibrahimi, A. P. Li, Z. Jiang, E. H. Conrad, C. Berger, C. Tegenkamp, and W. A. de Heer, "Exceptional ballistic transport in epitaxial graphene nanoribbons," Nature **506**(7488), 349–354 (2014).

#252250 Received 19 Oct 2015; revised 16 Nov 2015; accepted 16 Nov 2015; published 2 Dec 2015

1. Introduction

The plasmon induced transparency (PIT) effect, which generates a transparency window within a broad absorption spectrum, has attracted enormous attention because it's potentially important applications in the field of filters, sensors, and slow light [1]. The PIT effect is a plasmonic analogue of the electromagnetic induced transparency (EIT) effect, which is a strong destructive interference coupling phenomenon between a wideband bright mode and a narrowband dark mode [2]. Because of the ability provided by the surface plasmon polaritons (SPPs) to support modes with deep subwavelength scale and overcome classical diffraction limit, the devices based on PIT effect can be realized with small footprint [1,2]. Various plasmonic structures have been proposed to realize the PIT effect, e.g. metamaterials [3–6], plasmonic waveguide side-coupled with nanocavities (PWSCN) [7–13], metallic nanowire grating coupled with a dielectric waveguide layer [14, 15]. Among different plasmonic structures, the PWSCN structures are of special interest for the PIT effect can be obtained in the direction parallel to the device surface, which is benefit for on-chip plasmonic devices [5]. Recently, many plasmonic circuits require dynamically tunable PIT effect. However, once the devices are fabricated, active tuning of the PIT effect is very difficult to obtain. In recent years, graphene, a two-dimensional monolayer of carbon atoms, has been introduced to the field of plasmonics, such as plasmonic switches, filters, and sensors [16–19]. For example, Liu *et al.* proposed a tunable ultrasensitive platform for infrared and terahertz sensing based on the interaction between graphene surface plasmons (GSM) and molecules [19]. In contrast to the noble metal, the Fermi energy level of graphene can be flexibly tuned by gate voltage or chemical doping. This offers a tunable method to manipulate and confine SPPs with extremely high confinement and low propagation loss. For example, it has been demonstrated that the dynamically tunable PIT effect can be obtained in periodically patterned graphene nanostrips by altering the Fermi level of the graphene [20,21]. Moreover, the PIT effect also has been found in the graphene nanoribbon arrays [22], the heterogeneous graphene ribbon pairs [23], and the metamaterial structure which consists of a series of spatially separated graphene layers with different widths [24]. However, these configurations are difficult to integrate into on-chip plasmonic circuits. Furthermore, these devices also bring more challenges in fabrication because of the complicate structure.

To the best of our knowledge, graphene ribbon can support two kinds of SPPs modes: the waveguide mode and the edge mode [25–27]. A variety of tunable graphene waveguide devices have been proposed based on the waveguide mode, including switches [28], filters [29], and isolators [30]. More interestingly, when the width of graphene ribbon decreases to the order of nanometers, the waveguide mode vanishes and only the edge mode can exist on the rims of the graphene ribbons both vertically and laterally [25]. In recent years, much attention has been paid to the two-dimensional waveguide devices based on the lateral coupling between the graphene-based nanoribbon waveguide and graphene-based resonators. Compared with the photonics devices based on the waveguide mode, the devices based on the edge mode can be realized with smaller footprints. For example, it has been demonstrated that dynamically tunable plasmonic filters and Y-shape switches can be achieved in a graphene nanoribbon waveguide coupled with a graphene nanoring or a graphene nanodisk [31–33]. However, there are rarely related reports on the realization of dynamically tunable PIT effect in graphene nanoribbon waveguide structure based on the edge modes coupling.

Motivated by the above fundamental studies, we present dynamically tunable PIT effect in a graphene nanoribbon waveguide coupled with graphene rectangular resonators by shifting the Fermi levels of the graphene. Two different methods are employed to obtain the PIT effect: one is based on the near-filed coupling between a radiative state and a dark state, the other is based on the indirect coupling through a graphene-based nanoribbon waveguide. Besides, double PITs are also numerically predicted in this ultracompact structure, comprising series of graphene rectangular resonators. Compared with previously reported graphene-based PIT effects, our proposed structure is much easier to design and fabricate.

#252250 Received 19 Oct 2015; revised 16 Nov 2015; accepted 16 Nov 2015; published 2 Dec 2015

2. Model construction

Figure 1 schematically exhibits the proposed structures which consist of a graphene-based nanoribbon waveguide and series of graphene rectangular resonators. In order to support the edge modes, we select the width of the graphene-based nanoribbon waveguide as w = 10 nm and keep it fixed in the follow works [31]. Only the transverse magnetic (TM) polarized SPP modes which is injected from the left side is considered throughout this article. The substrate leakage should be an issue in the mid-infrared. Here, it should be noticed that the SiO_2 substrate is not suitable to support the graphene nanoribbons because of the strong absorption in the mid-infrared. As a result, the plasmonic waveguide and graphene rectangular resonators are deposited on a 50-nm-thick sapphire substrate. Li *et al.* have reported that the propagation loss of silicon-on-sapphire (SOS) waveguide is as low as 1.9dB/cm at 5.18 μm [34]. The characteristic spectral responses are calculated using the finite-difference time-domain (FDTD) (adopting commercial software *Lumerical* FDTD Solutions), and the perfectly matched layer (PML) conditions are used in the simulation [8, 21, 24, 31]. The substrate material is selected as Al_2O_3 (Palik) whose refractive index and extinction coefficient k are about 1.59 and 0.0020 at 6 μm, respectively [35]. To start with, a graphene-based nanoribbon waveguide coupled with single graphene rectangular resonator structure is shown in Fig. 1(a). In order to obtain PIT spectrum, another graphene rectangular resonator is added in the up or right side of the above single-resonator-coupled system to construct two-resonator-coupled system, as illustrated in Figs. 1(b) and 1(c), respectively. To obtain double-channel PIT effect, we also construct an ultracompact plasmonic structure which consists of a graphene-based nanoribbon waveguide and four graphene rectangular resonators, as shown in Fig. 1(d).

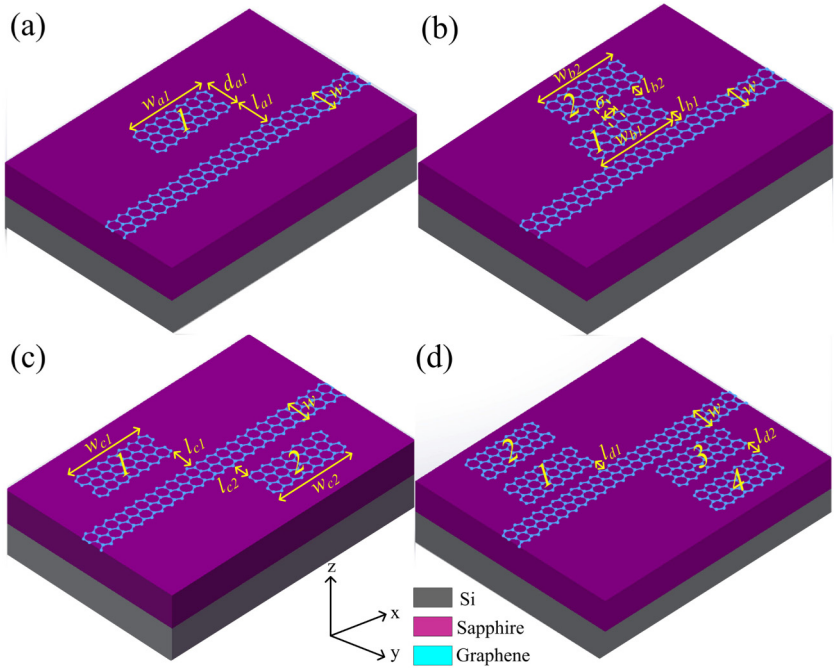

Fig. 1. Schematic diagram of the proposed one-resonator-coupled system (a), two-resonator-coupled system (b, c) and four-resonator-coupled system (d).

In contrast to the noble metal, the surface conductivity of graphene can be flexibly altering by chemical doping or gate voltage. In the mid-infrared range with $|\mu_c| >> k_B T$ and $\hbar\omega >> k_B T$, graphene's surface conductivity can be given by the Kubo formula [36]:

#252250 Received 19 Oct 2015; revised 16 Nov 2015; accepted 16 Nov 2015; published 2 Dec 2015

$$\sigma_{\mathrm{g}} = -i\frac{e^2 k_B T}{\pi\hbar^2\left(\omega + i\tau^{-1}\right)}\left[\frac{\mu_c}{k_B T} + 2\ln\left(\exp\left(-\frac{\mu_C}{k_B T}\right)+1\right)\right] - i\frac{e^2}{4\pi\hbar^2}\ln\left[\frac{2|\mu_c| - \hbar\left(\omega + i\tau^{-1}\right)}{2|\mu_c| + \hbar\left(\omega + i\tau^{-1}\right)}\right] \tag{1}$$

where e, $\hbar$, k_B, T and τ is the electron charge, the reduced Planck's constant, the Boltzmann's constant, the radian frequency, the temperature, and the relaxation time, respectively. The momentum relaxation time $\tau = \mu\mu_c / (ev_f^2)$ which depends on the direct current (DC) mobility μ, the chemical potential μ_c and the Fermi velocity v_f ($\approx 10^6$ m/s) is caused by charge carrier scattering. In recent years, it has been demonstrated that high-quality suspended graphene with $\mu > 10^5$ $\mathrm{cm^2V^{-1}s^{-1}}$ can be obtained experimentally, which leads to $\tau > 1.5$ ps [36]. It should be noted that a high relaxation time in graphene can reduce the transmission loss and thus obtain high transmittance in the transmission spectrum. However, it needs a high DC mobility in graphene which increases the difficulty in fabrication of the device undoubtedly. Here, we select the temperature $T = 300$ K and relaxation time $\tau = 1.0$ ps [36, 37]. Moreover, graphene's in-plane permittivity ε_{g} can be written as

$$\varepsilon_g = 1 + \frac{i\sigma_g \eta_0}{k_0 d_g} \tag{2}$$

where d_{g} (≈ 1 nm) is the thickness of monolayer graphene, η_0 (≈ 377 Ω) is the impedance of air, and k_0 is the wavevector in free space. Here, it should be noticed that graphene is anisotropic and the out-of-plane permittivity is set as 2.5 [22, 24]. In order to reduce the tremendous computation time in FDTD simulations, the mesh size inside the graphene layer is 0.2 nm, while non-uniform mesh size is employed to represent the other regions.

3. Results and discussions

In our simulations, the Fermi level of the graphene-based nanoribbon waveguide is constantly kept as 0.4 eV, and that of the graphene rectangular resonator is tuned by flexibly controlling the different gate voltages applied on the graphene [36]. The calculated transmission spectrum of the proposed single-resonator-coupled system for different chemical potentials is presented in Fig. 2(a). The edge modes considered here are excited by a dipole point source placed 250 nm away from the center of the graphene rectangular resonator in the x direction and there are 250 nm between the monitor and the center of the resonator [31]. The other parameters in this structure are assumed to be $l_{a1} = 15$ nm, $w_{a1} = 140$ nm, and $d_{a1} = 20$ nm. It should be noted that we can obtain the resonance wavelength for this single-resonators-coupled system based on the Fabry-Perot (FP) resonance condition [7]

$$\lambda = 2\,\mathrm{Re}(n_{eff}) \times L / (m - \varphi/\pi) \tag{3}$$

where φ is the phase shift brought by the SPPs reflection in the resonator, L is the effective length of the resonator, m is an integer. The waveguide effective refractive index n_{eff} can be obtained by solving the dispersion equation [29]

$$n_{eff} = \sqrt{1 - \left(\frac{2}{\eta_0 \sigma_g}\right)^2} \tag{4}$$

where η_0 (≈ 377 Ω) is the impedance of air. Based on the Eq. (1), (3), and (4), it's obvious that the resonance wavelength of the graphene resonator decreases as chemical potentials increases for a fixed length, and the calculated results are shown in Fig. 2(a). Obviously, when the structure parameters are assumed to be $\mu_c = 0.40$ eV, $l_{a1} = 15$ nm, $w_{a1} = 140$ nm,

#252250 Received 19 Oct 2015; revised 16 Nov 2015; accepted 16 Nov 2015; published 2 Dec 2015

and d_{a1} = 20 nm, the FWHM (full width at half maximums) of the transmission spectrum is about 160 nm, which exhibits band-stop filtering feature in the mid-infrared region. The inset in Fig. 2(c) shows the magnetic field distribution of 6786 nm when the chemical potential of the graphene resonator is set as 0.40 eV. It is obvious that the third-order resonance mode is supported by the graphene resonator. Notably, the insertion loss (IL) of the graphene waveguide is about 2.2 dB when the propagation length equals to 500 nm. The reason for this unnegligible loss is related to the propagation loss of the edge modes in graphene nanoribbion and the potential sapphire substrate leakage which is not considered in [31, 32]. Certainly, in order to reduce the potential substrate leakage, the operation wavelength can be adjusted to 5.3 μm by increasing the chemical potentials because the extinction coefficient k of sapphire substrate is about 0.0006 at 5.3 μm [35]. In addition, based on the Eq. (3), we also can find that the increase of length w_{a1} can result in the red shift of resonance wavelength for a fixed Fermi level, and the calculated results are shown in Fig. 2(b). Here, the Fermi level of the graphene resonator is set as 0.40 eV. Moreover, the coupling distance l_{a1} between the waveguide and graphene resonator also has an influence on the transmission dip and resonance wavelength. As shown in Fig. 2(c), as the coupling distance increases, the resonance wavelength of the resonator is red-shifted weakly and the depth of the transmission dip also decreases because of the weakening of the coupling strength between the waveguide and resonator. Furthermore, as shown in Fig. 2(d), as the width of the graphene resonator d_{a1} increases, the waveguide effective refractive index n_{eff} gets smaller, and it leads to the blue shift of the resonance wavelength. Obviously, our calculated results will benefit the realization of the planar, dynamically tunable, ultra-compact filters in the mid-infrared region.

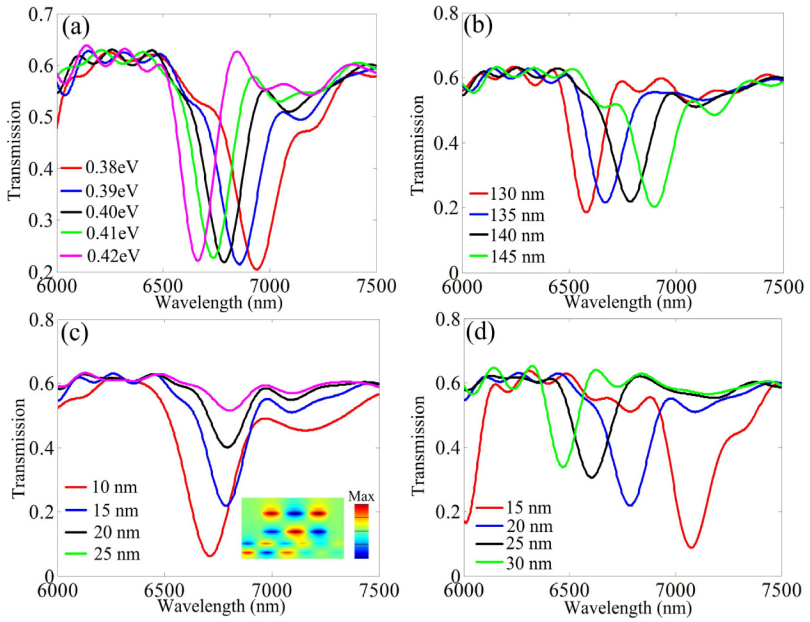

Fig. 2. Transmission spectrum of the proposed one-resonator-coupled structure shown in Fig. 1 (a) for different chemical potentials μ_c (a), lengths w_{a1} (b), coupling distances l_{a1} (c), and widths d_{a1} (d). The inset in (c) shows the magnetic field distribution of 6480 nm with other parameters are assumed to be μ_c = 0.40 eV, l_{a1} = 15 nm, w_{a1} = 140 nm, and d_{a1} = 20 nm.

Now let us come back to consider the two-resonator-coupled system as shown in Fig. 1(b). Figure 3(a) shows the calculated result when the centers of two graphene rectangular resonators match each other along the waveguide propagation direction. In other words, the lateral shift σ shown in Fig. 1(b) is set as 0 nm. The edge modes are excited by a dipole point source placed 200 nm away from the center of the 1st graphene rectangular resonator in the x direction. As expected, single PIT window is found in the transmission spectrum distinctly.

#252250 Received 19 Oct 2015; revised 16 Nov 2015; accepted 16 Nov 2015; published 2 Dec 2015

Here, we select the parameters l_{b1} = 15 nm, l_{b2} = 20 nm, μ_{b1} = 0.4 eV and μ_{b2} = 0.41 eV to construct a bright-dark resonator couple system. The 1st graphene rectangular resonator with length w_{b1} = 140 nm is directly side-coupled to the graphene-based nanoribbon waveguide, while the 2nd graphene rectangular resonator with w_{b1} = 140 nm is coupled to the 1st resonator. Obviously, the coupling strength between the 2nd rectangular resonator and graphene-based nanoribbon waveguide is weaker than that between the 1st resonator and waveguide. This makes the 1st resonator behave as a bright resonator and the 2nd resonator behave as a dark resonator [38]. It should be noticed that the graphene-based nanoribbon waveguide, the 1st graphene rectangular resonator and 2nd graphene rectangular resonator can be served as the bare element |1>, the dipole-allowed element |2> and the metastable element |3>, respectively [10]. There are two optical pathways $|1\rangle\rightarrow|2\rangle$ and $|1\rangle\rightarrow|2\rangle\rightarrow|3\rangle\rightarrow|2\rangle$ in our proposed two-resonator-coupled system. Namely, the 2nd graphene rectangular resonator can only be coupled to the 1st graphene rectangular resonator but cannot directly couple to the graphene-based waveguide. It's the destructive interference between the 1st bright resonator and 2nd dark resonator gives rise to transmission peaks B. As shown in Fig. 3 (h), distribution of the magnetic field corresponding transmission peak B confirms that the occurrence of this peak is related to the field suppression of the 1st graphene rectangular resonator. A temporal coupled mode theory (CMT) [37] and a radiation field model [13] has been introduced to explain the PIT effect in this bright-dark resonator couple model. Based on the CMT, the transmission spectrum can be expressed as [37]

$$T(\lambda) = 1 - \frac{1}{1 + [\lambda - \lambda_1 - |\kappa_2|^2/(\lambda - \lambda_2)]^2 / |\kappa_1|^2} \tag{5}$$

where λ_1 and λ_2 denote the resonance wavelengths of the 1st bright resonator and 2nd dark resonator, respectively, κ_1 represents the coupling coefficient between the waveguide-bright resonator coupling, κ_2 represents the coupling coefficient between the bright-dark resonators coupling.

It is widely recognized that the different coupling distance l_{b2} between the bright and dark resonators can influence the transparency window. Figure 3(b) presents the transparency window when the coupling distance l_{b2} is increased from 20 nm to 35 nm with a step of 5 nm. It should be noticed that the increase of the coupling distance l_{b2} can result in lower transmission peak and narrower bandwidth. The reason for this phenomenon is that the increase of coupling distance l_{b2} weakens the coupling strength between the bright and dark graphene rectangular resonator. Moreover, the dynamically tunability of PIT effect is shown in Fig. 3(c). Here, the Fermi level of the 1st graphene rectangular resonator is constantly kept as μ_{b1} = 0.40 eV, while the Fermi level of the 2nd graphene rectangular resonator are set as different values μ_{b2} = 0.39, 0.40, 0.41, and 0.42 eV, respectively. As shown in Fig. 3(c), as the Fermi level μ_{b2} increases, the transmission peak in the PIT transparency window is blue-shifted obviously. As a result, the dynamically tunable PIT effect can be achieved in our proposed structure by altering the Fermi level of the 2nd graphene resonator. Figure 3(d) exhibits the transmission spectrum when the lateral shift σ is increased from 0 to 25 nm with a step of 5 nm. It is obvious that as lateral shift σ increases, the transmission peak of the transparency window drops, demonstrating that the coupling strength between the 1st resonator and 2nd resonator gets weaker. It should be noticed that the structural defects of graphene nanoribbons (GNRs) can strongly impact the electrical transport properties of graphene [39]. This happened, for example, in fabrication using electron-beam lithography followed by oxygen plasma etching, which yields GNRs with rough edges and defects [39]. We calculate the transmission spectrum for the two-resonator-coupled system with different relaxation times τ = 0.5, 0.4, 0.3, 0.2, 0.1 and 0.06 ps, and the results are shown in Fig. 3(e). Here, the distance between the source and monitor is set as 200 nm. It is obvious that a PIT transmission window grows in strength and becomes prominent as τ increases from 0.1 to 0.5 ps. These results clearly show that decreasing τ will result in a lower value of the transmission spectrum because of the larger propagation loss. Moreover, when τ = 0.1 ps, it can be clearly

#252250 Received 19 Oct 2015; revised 16 Nov 2015; accepted 16 Nov 2015; published 2 Dec 2015

seen from Fig. 3(e) that there also exists an obvious transmission window although the transmission contrast between the optical channel and the stop band is small. To further illustrate the influence of relaxation times, the evolution of transmission spectrum verses τ and λ is numerically calculated and presented in Fig. 3(f). It is

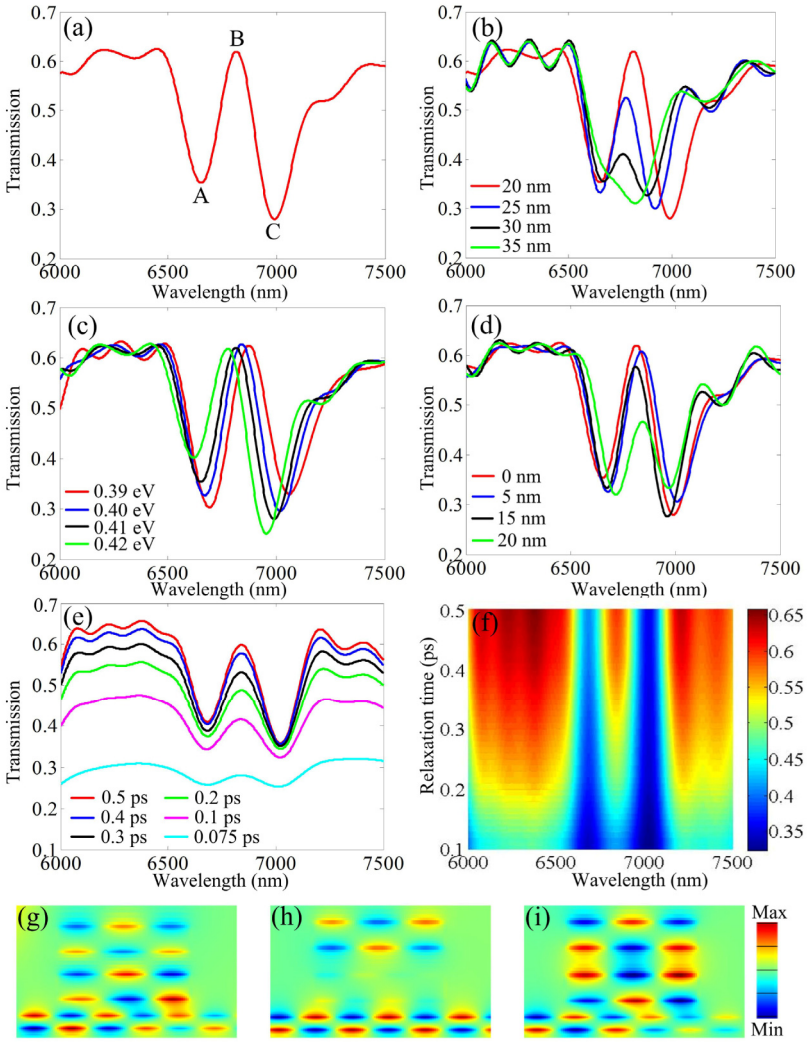

Fig. 3. (a) Transmission spectrum of the proposed two-resonator-coupled structure shown in Fig. 1 (b) with l_{b1} = 15 nm, l_{b2} = 25 nm, w_{b1} = w_{b2} = 140 nm, μ_{b1} = 0.4 eV, μ_{b2} = 0.41 eV. Transmission spectrum of the system for different coupling distances l_{b2} (b), chemical potentials μ_{b2} (c), lateral shifts σ (d), and relaxation times of graphene (e). (f) Evolution of transmission spectrum verses τ and λ. (g)-(i) Distributions of the magnetic field corresponding to the two transmission dips and the one transmission peak represented by A, C, and B in (a).

found that there exists one well-pronounced transmission peak between two transmission dips. One can see that as relaxation time decreases the transmittance drops and the transmission contrast becomes smaller. We also calculate the transmission spectrum for nano-patterned VCD graphene with relaxation time τ = 0.075 ps ($\mu \approx 1800$ cm^{2}V^{-1}s^{-1}) which is in good accordance with experimental data produced by conventional lithographic processing. It can be found that an inconspicuous PIT effect emerges in the forbidden band and the transmittance and transmission contrast drop dramatically when the relaxation time τ is

#252250 Received 19 Oct 2015; revised 16 Nov 2015; accepted 16 Nov 2015; published 2 Dec 2015

changed from 0.1 to 0.075 ps. It means that a relatively low relaxation time ($\tau < 0.1$ ps) has profound effects on the performance and produces a problem that perfect PIT effect is difficult to obtain. Obviously, in order to obtain pronounced PIT effect in this two-resonator-coupled system, the relaxation time of graphene should be more than 0.1 ps ($\mu > 2500$ $cm^2V^{-1}s^{-1}$). Besides, the edge modes of graphene are sensitive to edge defects of GNRs. Except for the low carrier mobility induced by structural defects, if the edge modes are excited on the rough edge, it is expected that the large propagation loss and low transmittance can be obtained. Obviously, it is necessary to control the defects formation and edge roughness of GNRs in the nano-patterning process. Some important progress in this problem has been reported recently. Xu *et al.* used the STEM electron beam to sculpt GNRs and could pattern GNRs with sub-nanometer accuracy [40]. A recent experiment by Qi *et al.* showed atomically smooth GNRs with superior electrical transport could be obtained by increasing application of Joule heating, which facilitated atomic recrystallization and reduced the density of defects [41]. Baringhaus *et al.* pointed out that exceptional ballistic transport in GNRs could be obtained and these GNRs had well-defined edge orientations and were mostly defect-free, which indicated that a high carrier mobility ($\mu > 10000$ $cm^2V^{-1}s^{-1}$) can be obtained [42]. In conclusion, it is expected that the smooth and mostly free-defect GNRs with relatively large carrier mobility can be achieved in the nano-patterning process.

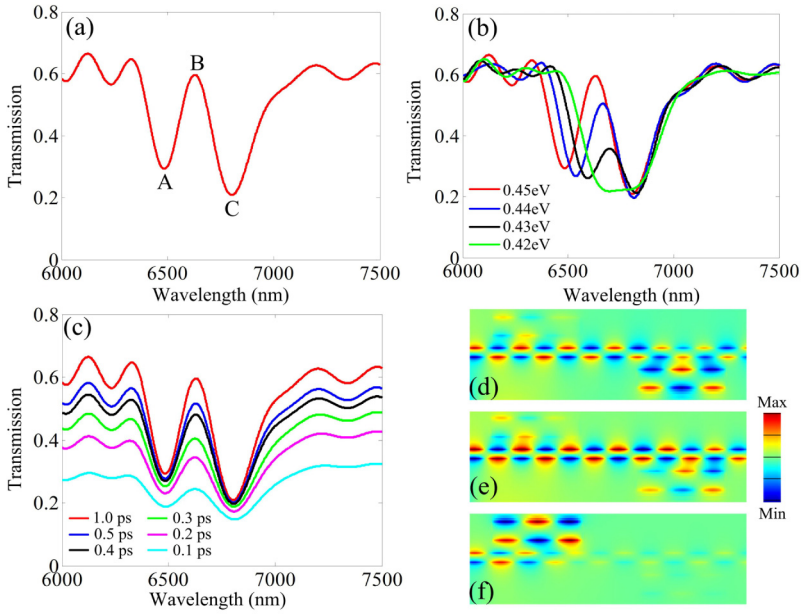

Fig. 4. (a) Transmission spectrum of the proposed two-resonator-coupled structure shown in Fig. 1 (c) with $l_{c1} = l_{c2} = 15$ nm, $w_{c1} = w_{c2} = 140$ nm, $\mu_{c1} = 0.4$ eV, $\mu_{c2} = 0.45$ eV. (b)-(c) Transmission spectrum of the system for different chemical potentials μ_{c2} and relaxation times τ. (d)-(f) Distributions of the magnetic field corresponding to the two transmission dips and transmission peak represented by A, B, and C in (a).

Next let us consider the two-resonator-coupled system as shown in Fig. 1(c). It should be noted that the structure shown in Fig. 1(c) is quite different from that in Fig. 1(b). In Fig. 1(c), two side-coupled graphene rectangular resonators with a center-to-center distance (160 nm) are placed in the opposite side of the graphene-based nanoribbon waveguide. Here, the distance between the source and monitor is set as 400 nm. For simplicity, the coupling distances between the graphene resonators and waveguide are constantly kept as $l_{c1} = l_{c2} = 15$ nm, and the lengths of the resonators are set as $w_{c1} = w_{c2} = 140$ nm. In order to obtain the PIT effect, the Fermi levels of the graphene rectangular resonator are assumed to be $\mu_{c1} = 0.4$ eV, $\mu_{c2} = 0.45$ eV, respectively. As shown in Fig. 2 (a), different Fermi levels of the graphene

#252250 Received 19 Oct 2015; revised 16 Nov 2015; accepted 16 Nov 2015; published 2 Dec 2015

rectangular resonator can lead to different resonant wavelengths. It has been demonstrated that if two resonators with certainly different resonant wavelengths are placed in the opposite side of the waveguide, the PIT effect can show up in the transmission spectrum [7–9]. Therefore, the PIT effect can be found in the transmission spectrum distinctly, as shown in Fig. 4 (a). It should be noticed that the reason for the occurrence of the transmission peak B in Fig. 4 (a) is quite different from that in Fig. 3 (a). It's the near-filed coupling between the 1st bright resonator and the 2nd dark resonator gives rise to transmission peaks B in Fig. 3 (a). However, the occurrence of the transmission peak in Fig. 4 (a) is related to the destructive interference between two detuned dipoles through the graphene-based nanoribbon waveguide [7–9]. The appearance of the transmission peaks B can be confirmed in the magnetic field distribution shown in Fig. 4 (e). In addition, dynamically tunability of transparency window is also achieved by altering the Fermi level of the 2nd graphene resonator, and the calculated results are shown in Fig. 4 (b). Here, the Fermi level of the 1st graphene resonator is assumed to be μ_{c1} = 0.40 eV. Therefore, the transmission dip C remains the same approximately, while the transmission dip A is blue-shifted when the Fermi level of the 2nd resonator increases from 0.42 to 0.45 eV. In addition, we also consider the influence of relaxation times on the PIT effect in this system. The calculated result shown in Fig. 4(c) is similar with that in Fig. 3(e): a PIT transmission window grows in strength and becomes prominent as τ increases from 0.1 to 0.5 ps. However, when τ = 0.1 ps, an inconspicuous PIT effect emerges in the forbidden band and the transmittance of PIT effect is smaller than that shown in Fig. 3(e). The reason for this phenomenon is attributed to that the propagation distance of the two-resonator-coupled system shown in Fig. 1(c) is longer that that in Fig. 1(b).

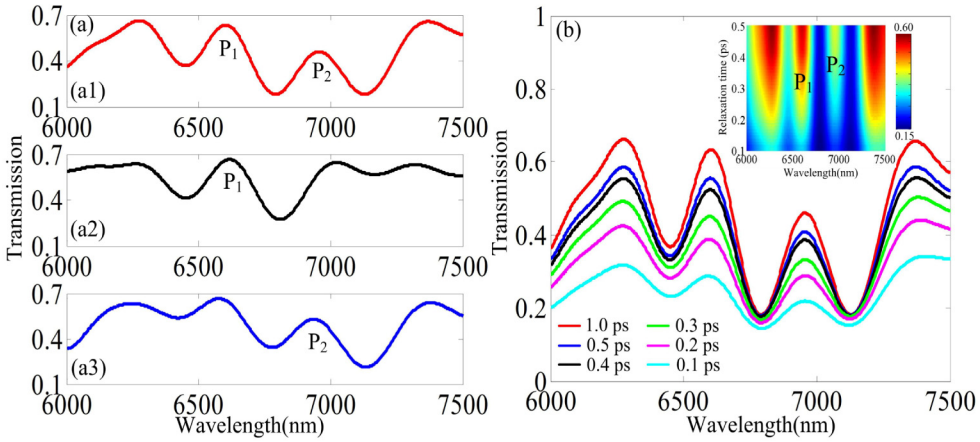

Fig. 5. (a) Transmission spectrum of the proposed four-resonator-coupled structure with l_{d1} = 15 nm, l_{d2} = 20 nm, μ_{d1} = 0.38 eV, μ_{d2} = 0.39 eV, μ_{d3} = 0.43 eV, and μ_{d4} = 0.44 eV. Transmission spectrum of the system when only the 1st, 2nd resonators (a2) and the 3rd, 4th resonators (a3) are placed on one side of the graphene waveguide. (b) Transmission spectrum for different relaxation times. Inset is the evolution of transmission spectrum verses τ and λ.

Many plasmonic circuits require multiple-channel PIT transparency windows. Figure 5(a) exhibits the calculated transmission spectrum of the proposed four-resonator-coupled system shown in Fig. 1(d). Here, the lengths and widths of all graphene rectangular resonators are constantly kept as 140 nm and 20 nm, respectively. The distance between the source and monitor is set as 400 nm. The center-to-center distance between the 1st and 3rd graphene resonator is set to be 120 nm. The coupling distance between the 1st (3rd) graphene resonator and graphene-based nanoribbon waveguide is set as l_{d1} = 15 nm. In contrast, the 2nd (4th) resonator is placed on a suitable position (l_{d2} = 20 nm) where the 2nd (4th) resonator can't directly couples with the graphene waveguide but can be coupled to the 1st (3rd) graphene resonator. In order to obtain PIT effect, the Fermi levels of the 1st, 2nd, 3rd, and 4th graphene rectangular resonators are set as 0.38, 0.39, 0.43, and 0.44 eV, respectively. As shown in Fig.

#252250 Received 19 Oct 2015; revised 16 Nov 2015; accepted 16 Nov 2015; published 2 Dec 2015

5(a1), double optical channels obviously emerge in the forbidden band and transmission peaks of 0.63 and 0.46 are achieved at wavelengths 6630 nm and 6956 nm, respectively. In order to get more insight into the physics of the double PIT responses observed, we study a simple structure in which there are only two graphene rectangular resonators on one side of the graphene waveguide, rather than the whole structure as shown in Fig. 1 (d). Figures 5(a2) and 5(a3) show the transmission spectrums of the system when only the 1st, 2nd resonators and the 3rd, 4th resonators are placed on one side of the graphene waveguide, respectively. It can be noticed that single PIT effect emerges in the transmission spectrum distinctively. It means that the reason for the occurrence of the transmission peak A (B) in Fig. 5(a1) is related to the destructive interference between the 1st (3rd) bright resonator and the 2nd (4th) dark resonator. We also consider the influence of different relaxation times on this four-resonator-coupled system. When the relaxation time of graphene increases from 0.1 to 0.5 ps, the transmittance of optical channel 1 (optical channel 2) at central wavelength is changed from 0.58 (0.46) to 0.27 (0.22) correspondingly. Inset in Fig. 5(b) is the transmission evolution as a function of relaxation time for this structure. It is found that double optical channel (P_1 and P_2) obviously emerge in the forbidden band and as relaxation time decreases the transmittance of the optical channel drops. In conclusion, in order to obtain pronounced PIT effects in this structure, the relaxation time of graphene should be more than 0.2 ps ($\mu >$ 5000 $cm^2V^{-1}s^{-1}$) because of the long propagation distance.

4 Conclusions

In conclusion, we propose dynamically tunable PIT effect in a graphene nanoribbon waveguide coupled with graphene rectangular resonators on sapphire substrate by shifting the Fermi levels of the graphene. In this article, two different realization methods are employed to obtain the PIT effect: one is based on the near-filed coupling between a radiative resonator and a dark resonator, the other is based on the indirect coupling through a graphene-based nanoribbon waveguide. Besides, double PITs are also numerically predicted in this ultracompact structure, comprising series of graphene rectangular resonators. Compared with previously reported graphene-based PIT effects, our proposed structure is much easier to design and fabricate. This work not only paves a new way towards the realization of graphene-based integrated nanophotonic devices, but also has important applications in multi-channel-selective filters, sensors, and slow light.

Acknowledgment

This work is supported by the National Natural Science Foundation of China (Grant No. 61376055 and 61006045), and the National Basic Research Program of China (Grant No. 2010CB923204).

#252250 Received 19 Oct 2015; revised 16 Nov 2015; accepted 16 Nov 2015; published 2 Dec 2015